Nanoscale

COMMUNICATION

View Article Online
View Journal | View Issue

Check for updates

Cite this: *Nanoscale*, 2024, **16**, 12420

Received 13th April 2024,
Accepted 5th June 2024

DOI: 10.1039/d4nr01619j

rsc.li/nanoscale

Published on 05 2024. Downloaded on 01.06.26 19:16:31.

An organophosphate 3d–4f heterometallic polyoxoniobate nanowire†

Jin-Ai Fan,‡[a] Hao Yu,‡[a] Yu-Diao Lin,[a,b] Ming-Qiang Qi,[c] Xiang-Jian Kong,[c] Cai Sun *[a] and Shou-Tian Zheng *[a]

Four different structural compositions of organophosphate, 3d transition metal, 4f lanthanide and polyoxoniobate (PONb) are unified in a system for the first time to form a new type of organophosphate 3d–4f heterometallic inorganic–organic hybrid PONb nanowire. Interesting magnetic anisotropy and slow magnetic relaxation are found in the PONb nanowire.

Polyoxometalates (POMs) typically refer to a class of cluster structures assembled from high-valent transition metals V, Mo, W, Nb, and Ta with oxygen atoms. By virtue of their controllable structures by introducing heterometallic ions, POMs have potential applications in optics, magnetism, catalysis, and functional materials and have attracted the attention of numerous researchers.[1] The introduction of 3d transition metals and 4f lanthanides in POMs can form 3d transition metal-substituted polyoxometalates (3d POMs) and 4f lanthanide-substituted polyoxometalates (4f POMs), respectively.[2,3] To date, extensive studies with rich applications has documented research on 3d POMs and 4f POMs.[4] Furthermore, 3d–4f heterometallic POMs (3d–4f POMs) exhibit unique configurations, superior physicochemical properties, and intriguing synergistic interactions between transition metals and lanthanide metals, sparking researchers' interest in exploring their potential applications in emerging technologies.[5] However, the development of 3d–4f POMs lags significantly behind 3d POMs and 4f POMs.[6]

Until now, reports on 3d–4f heterometallic substituted POMs have focused on polyoxotungstates (POWs) and polyoxomolybdates (POMos)[7] such as two giant 3d–4f POW clusters $[LaNi_{12}W_{35}Sb_3P_3O_{139}(OH)_6]^{23-}$ and $[La_{10}Ni_{48}W_{140}Sb_{16}P_{12}O_{568}(OH)_{24}(H_2O)_{20}]^{86-}$ from Kong group[8] two new classes of highly reduced mix-valence 3d–4f POMos $[Mo_{64}Ni_8Ln_6H_{26}O_{200}(H_2O)_{30}]^{8-}$ from Cronin group.[9] In contrast, the development of 3d–4f heterometallic substituted polyoxoniobate (PONb) remains a challenge. Firstly, the lack of soluble niobate oxoanion precursors, low activity and the narrow working pH region ranging 10–12 of niobate species are major limiting factors for the synthesis of PONbs.[10] Secondly, alkaline working pH triggers the hydrolysis of lanthanides and transition metal ions, leading to the precipitation of oxide compounds. Thirdly, the different oxophilicity of 4f lanthanides and 3d transition metals inevitably lead to a competitive reaction, making it difficult to connect to PONb clusters simultaneously.[11]

Recently, we found that the hydrolysis of lanthanide ions in alkaline environments can be effectively restrained through the synergistic coordination of an organophosphate and a sodium carbonate buffer system and enabled the successful construction of a series of organophosphate–Ln–PONb composite clusters.[12] Building upon the knowledge acquired in our previous studies, we are very interested in the challenge of synthesizing the PONb with 3d and 4f metal ions simultaneously and developing a research area that holds great potential for advancement.

Herein, four different structural compositions of organophosphate, 3d transition metal, 4f lanthanide and PONb are unified in a system for the first time, forming a new type of organophosphate 3d–4f heterometallic inorganic–organic hybrid PONb nanowire, denoted as: $H_{33}K_{18}Na_5\{[Co(H_2O)_4]_2[Dy_4(CO_3)_4(EA)_2]_2[Nb_{32}O_{92}(H_2O)_4]_2\}\cdot 104H_2O$ (**1**, EA = etidronic acid). The successful realization of **1** demonstrates the possibility of fusing four separate research areas of PONb chemistry, lanthanide chemistry, transition metal chemistry, and organophosphate chemistry. Such a multi-component system can lead to great compositional and topological diversity, showing a general strategy toward the construction of rich organophosphate–TM–Ln–PONb composite clusters.

[a]*Fujian Provincial Key Laboratory of Advanced Inorganic Oxygenated Materials, College of Chemistry, Fuzhou University, Fuzhou, Fujian 350108, China. E-mail: csun@fzu.edu.cn, stzheng@fzu.edu.cn*
[b]*Fujian Provincial Key Laboratory of Coastal Basin Environment, Fujian Polytechnic Normal University, Fuqing, Fujian 350300, China*
[c]*State Key Laboratory of Physical Chemistry of Solid Surface, College of Chemistry and Chemical Engineering, Xiamen University, Xiamen, 361005, China*

†Electronic supplementary information (ESI) available. CCDC 2327331. For ESI and crystallographic data in CIF or other electronic format see DOI: https://doi.org/10.1039/d4nr01619j

‡These authors contributed equally to this work.

This journal is © The Royal Society of Chemistry 2024

Published on 05 2024. Downloaded on 01.06.26 19:16:31.

PONb **1** was synthesized by reacting Lindqvist-type PONb precursor $K_7HNb_6O_{19}{\cdot}13H_2O$ with $Dy(Ac)_3{\cdot}6H_2O$, cobalt acetylacetonate and EA in a $Na_2CO_3/NaHCO_3$ buffer solution (pH 11.5) and 80 °C for 3 days (see the Experimental section in the ESI†). Powder X-ray diffraction (PXRD) patterns indicate that as-synthesized crystalline samples had a pure phase (Fig. S1†). The water content in the crystal was determined by thermogravimetric analysis (Fig. S2†).

Single-crystal X-ray diffraction analyses revealed that **1** crystallizes in triclinic space group $P\bar{1}$ and its crystallographic data and structure refinement are summarized in Table S1.† As shown in Fig. 1a, the polyoxoanion $\{[Dy_4(CO_3)_4(EA)_2]_2[Nb_{32}O_{92}(H_2O)_4]_2\}$ (Dy_8Nb_{64}) as a secondary building unit (SBU) is constructed by two $\{\gamma\text{-}Nb_{32}O_{92}(H_2O)_4\}$ ($\gamma\text{-}Nb_{32}$) fragments joined together with two mutually centrosymmetric $[Dy_4(CO_3)_4(EA)_2]_2$ motifs and displays an interesting sandwich-like arrangement. $\gamma\text{-}Nb_{32}$ is a classical four-membered cyclic PONb macrocyclic fragment, the structural details of three types of Nb_{32} fragments (α-, β-, γ-), which have been discussed in detail in our previous work,[12] ultimately differ in size and symmetry due to the difference in the connection of the central Nb_8 ring and the distribution position of the peripheral Nb_6 cluster blocks (Fig. S5†).

The $[Dy_4(CO_3)_4(EA)_2]$ motif consists of four regular DyO_8 bicapped trigonal prisms that are connected in a corner-sharing fashion, which are constructed with four oxygen atoms provided by two CO_3^{2-}, two oxygen atoms provided by an EA ligand, with the remaining coordination site occupied by two terminal oxygen atoms stem from $\gamma\text{-}Nb_{32}$. The four Dy^{III} ions form a square plane with two pairs of CO_3^{2-} ions arranged orthogonally above and below the square plane. The CO_3^{2-} ions are encapsulated by Dy_4 and connected to two Dy^{III}

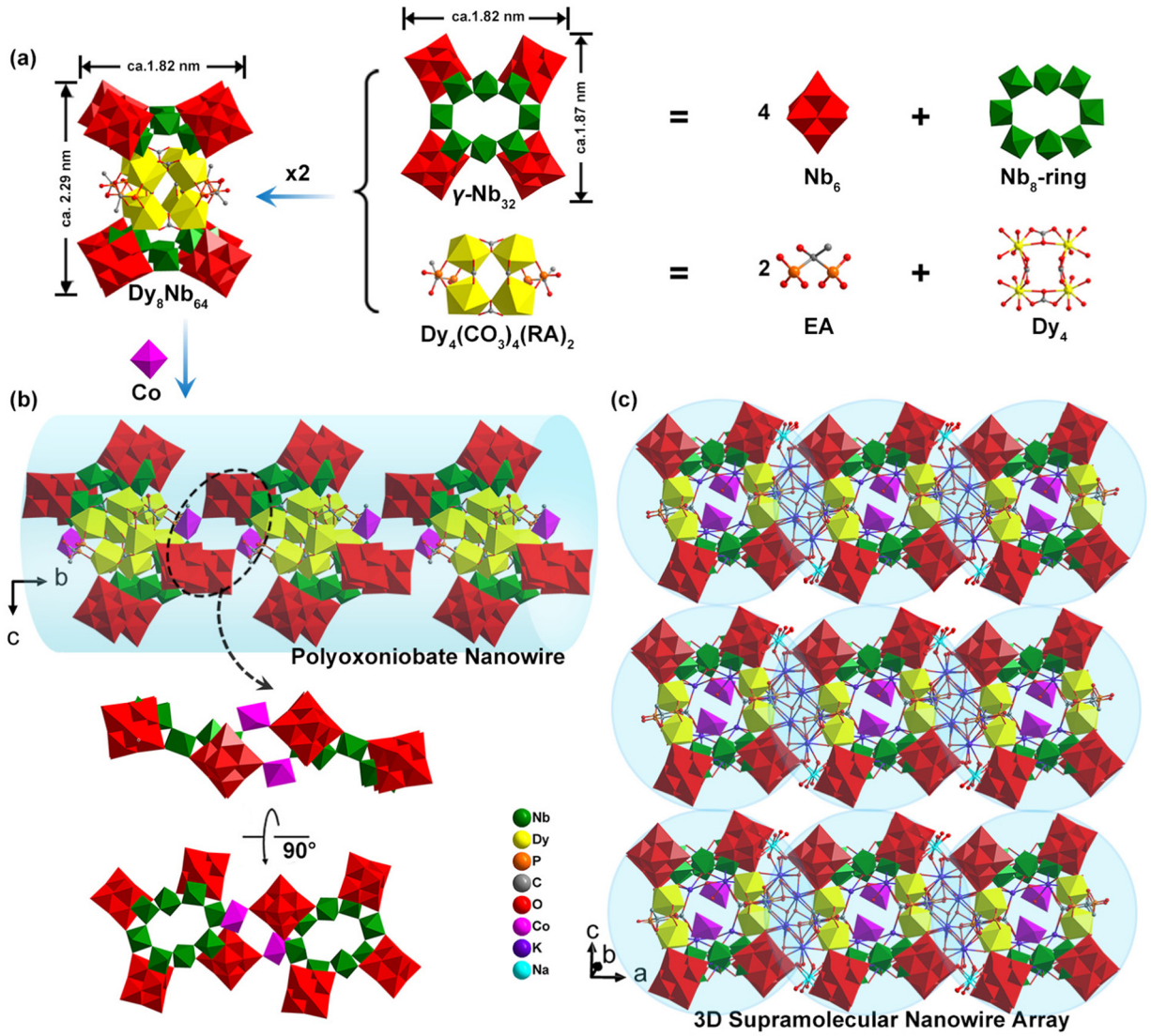

Fig. 1 Structure of **1**. (a) Dy_8Nb_{64} cluster; $\gamma\text{-}Nb_{32}$ cluster; Dy_4 cluster. (b) Representation of the 1D polyoxoanion of **1**. Localized schematic of Co^{II} linking **1** into a nanowire. (c) View of the 3D supramolecular nanowire array. NbO_6 octahedra: red/green; DyO_8 square antiprism: yellow; CoO_6 octahedra: pink.

Published on 05 2024. Downloaded on 01.06.26 19:16:31.

ions through the two two-coordinated oxygen atoms and one three-coordinated oxygen atom. The Dy_4 clusters are further linked by two EA ligands positioned at opposing edges of the square, where each EA ligand is connected to two Dy^{III} ions through two phosphonic acid groups. Additionally, two $[Dy_4(CO_3)_4(EA)_2]$ motifs are embedded in a sandwich formed by two opposing γ-Nb_{32} clusters. Each $[Dy_4(CO_3)_4(EA)_2]$ motif is linked with NbO_6 octahedra *via* eight Dy–O═Nb bonds [Dy–O bonds, 2.267(2)–2.498(3) Å; Nb═O bonds, 1.715(3)–2.466(2) Å]; Fig. 1a, generating a huge inorganic–organic hybrid three-layered PONb SBU-like "hamburger" with the dimensions of *ca.* 2.29 × 1.87 × 1.82 nm^3. The oxidation states of all Nb, Co and Dy atoms in **1** were confirmed as +5, +2 and +3 by Bond Valence Sum calculations (Tables S2–S4†).

Interestingly, each SBU is linked to adjacent one by two Co-centered distorted octahedra $[CoO_6]$ to give a 1D nanowire along the *b* direction, where each Co^{II} linker is coordinated by four water ligands and two terminal Nb═O oxo atoms (Co–O bonds: 2.094(7)–2.289(8) Å) (Fig. 1b and S6–S8†). The two Nb═O oxo atoms stem from Nb_6 and Nb_8-ring at the top and bottom of the adjacent SBUs, respectively. Finally, the 1D PONb nanowires further give rise to a 3D supramolecular nanowire array (Fig. 1c) through hydrogen bonds and electrostatic interactions between the hydrated sodium and potassium complex.

Motivated by the spin of Co^{II}, high spin–orbit coupling of Dy^{III}, and their possible magnetic interactions, we explored the magnetic properties of **1**. Firstly, the direct current (DC) magnetic susceptibility (χ_m) of **1** was measured at an external magnetic field of 0.1 T with a temperature range of 2–300 K. The plots of χ_mT *vs.* *T* are shown in Fig. 2a, the observed χ_mT value at 300 K for **1** is 113.68 cm^3 K mol^{-1}, which is slightly lower than the theoretical value of 117.11 cm^3 K mol^{-1} calculated for eight Dy^{3+} ions (14.17 cm^3 K mol^{-1}) and two Co^{2+} (1.875 cm^3 K mol^{-1}), probably resulting from weak antiferromagnetic interactions within the nanochain.[14,15] As the temperature drops, the χ_mT value drops smoothly from 300 K to 100 K and declines rapidly to a minimum of 71.23 cm^3 K mol^{-1} at 2 K. The result indicates the presence of magnetic anisotropy of the isolated Co^{II} and Dy^{III} ions or antiferromagnetic coupling interactions between adjacent Dy^{III} ions.[13] The field-dependent isothermal magnetization (*M*) of **1** was investigated at 2 K with the field strength (*H*) varying from 0 T to 8 T. Fig. 2b shows the rapid increase in *M* values at low fields, reaching 38.53*Nβ* at 1 T under 2 K, then followed by a slight rise to a maximum value of 44.57*Nβ*, which is less than the predicted saturation value of 86*Nβ*. This is most likely due to the large magnetic anisotropy or crystal-field effects at the Dy^{III} ions, eliminating the 16-fold degeneracy of the $^6H_{15/2}$ ground state.[16]

Furthermore, the combined effect of 3d–4f interactions can enhance the properties of a single molecule magnet.[17] To study the dynamic properties of **1**, alternating-current (AC) magnetic susceptibilities were investigated with frequencies ranging from 311 to 2311 Hz under an applied magnetic field of 3 Oe and zero direct-current fields. Notably, the observed out-of-phase (χ''_m) signals of **1** show frequency dependence with the varying frequency, and clearly indicate a slow magnetic relaxation below 10 K (Fig. 2c and d). The behavior of **1** aligns with the Debye model, characterized by one energy barrier and one-time constant based on the relationship: $\ln(\chi''_m/\chi'_m) = \ln\omega\tau_0 + U_{eff}/T$,[18] which allows for a rough estimation of the energy barrier of the relaxation process (Table S5 and Fig. S9†). The smaller energy barrier of the slow magnetic relaxation may be caused by quantum tunneling.

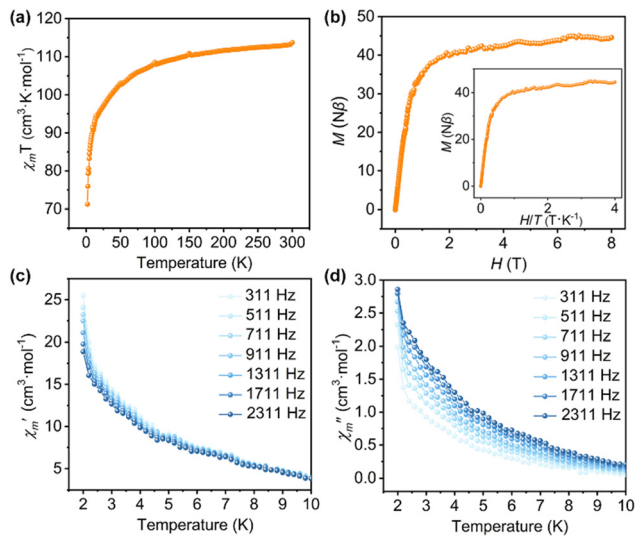

Fig. 2 For **1**. (a) Temperature-dependence of χ_mT in the temperature range of 2–300 K; (b) field-dependence of magnetization at 2 K. Inner: *M vs. H*/*T* plots. (c and d) Temperature-dependent behavior of the in-phase (χ'_m) and out-of-phase (χ''_m) in zero static fields at 2–10 K.

Conclusions

In summary, we successfully obtained an organophosphate 3d–4f heterometallic inorganic–organic hybrid PONb nanowire, unifying organophosphate, 3d transition metal, 4f lanthanide and PONb in a system for the first time. This hybrid PONb not only exhibits significant magnetic anisotropy but also demonstrates a noticeable slow magnetic relaxation. This work opens avenues for further exploration in the realm of multicomponent functional PONb.

Conflicts of interest

There are no conflicts to declare.

Acknowledgements

This work was supported by the National Natural Science Foundation of China (22371045, 22371046), Fujian Natural Science Youth Innovation Project (2021J05111, 2023J05211), Fujian Provincial Chemistry Discipline Alliance Foundation (50025401).

This journal is © The Royal Society of Chemistry 2024

Published on 05 2024. Downloaded on 01.06.26 19:16:31.

Notes and references

1 (*a*) B. Qin, H. Y. Chen, H. Liang, L. Fu, X. F. Liu, X. H. Qiu, S. Q. Liu, R. Song and Z. Y. Tang, *J. Am. Chem. Soc.*, 2010, **132**, 2886–2888; (*b*) Y. D. Lin, R. Ge, C. B. Tian, C. Sun, Y. Q. Sun, Q. X. Zeng, X. X. Li and S. T. Zheng, *Chem. Commun.*, 2021, **57**, 8624; (*c*) N. Li, J. Liu, B. X. Dong and Y. Q. Lan, *Angew. Chem., Int. Ed.*, 2020, **59**, 20779–20793; (*d*) X. M. Luo, N. F. Li, Z. B. Hu, J. P. Cao, C. H. Cui, Q. F. Lin and Y. Xu, *Inorg. Chem.*, 2019, **58**, 2463–2470.

2 (*a*) Z. W. Guo, L. H. Lin, J. P. Ye, Y. Chen, X. X. Li, S. Lin, J. D. Huang and S. T. Zheng, *Angew. Chem., Int. Ed.*, 2023, **62**, e202305260; (*b*) S. S. Zhang, O. Oms;, L. Hao, R. J. Liu, M. Wang, Y. Q. Zhang, H. Y. He, A. Dolbecq, J. Marrot, B. Keita, L. J. Zhi, P. Mialane, B. Li and G. J. Zhang, *ACS Appl. Mater. Interfaces*, 2017, **9**, 38486–38498; (*c*) J. Zhen, W. Y. Wang, R. Wan, X. Y. Ma, Y. Y. Qiao, Y. F. Bai, P. T. Ma, J. Y. Niu and J. P. Wang, *Inorg. Chem.*, 2022, **61**, 16528–16532.

3 S. M. Liu, Z. Zhang, X. H. Li, H. J. Jia and S. X. Liu, *J. Alloys Compd.*, 2018, **761**, 52–57.

4 (*a*) G. Y. Zhang, F. Wang, T. Tubul, M. Baranov, N. Leffler, A. Neyman, J. M. Poblet and I. A. Weinstock, *Angew. Chem., Int. Ed.*, 2022, **61**, e202213162; (*b*) Z. K. Zhu, Y. Y. Lin, R. D. Lai, X. X. Li, Y. Q. Sun and S. T. Zheng, *Chin. Chem. Lett.*, 2023, **34**, 107773; (*c*) D. D. Li, P. T. Ma, J. Y. Niu and J. P. Wang, *Coord. Chem. Rev.*, 2019, **392**, 49–80; (*d*) C. Boskovic, *Acc. Chem. Res.*, 2017, **50**, 2205–2214.

5 (*a*) Y. N. Gu, Y. Chen, Y. L. Wu, S. T. Zheng and X. X. Li, *Inorg. Chem.*, 2018, **57**, 2472–2479; (*b*) M. Ibrahim, V. Mereacre, N. Leblanc, W. Wernsdorfer, C. E. Anson and A. K. Powell, *Angew. Chem., Int. Ed.*, 2015, **54**, 15574–15578; (*c*) Y. H. Chen, L. H. Sun, S. Z. Chang, L. J. Chen and J. W. Zhao, *Inorg. Chem.*, 2018, **57**, 15079–15092.

6 V. Das, R. Kaushik and F. Hussain, *Coord. Chem. Rev.*, 2020, **143**, 213271.

7 (*a*) Y. N. Gu, H. Yu, L. D. Lin, Y. L. Wu, Z. Li, W. Y. Pan, J. He, L. Chen, Q. Li and X. X. Li, *New J. Chem.*, 2019, **43**, 3011–3016; (*b*) E. Tanuhadi, E. Al-Sayed, G. Novitchi, A. Roller, G. Giester and A. Rompel, *Inorg. Chem.*, 2020, **59**, 8461–8467; (*c*) J. Cai, X. Y. Zheng, J. Xie, Z. H. Yan, X. J. Kong, Y. P. Ren, L. S. Long and L. S. Zheng, *Inorg. Chem.*, 2017, **56**, 8439–8445.

8 S. R. Li, H. Y. Wang, H. F. Su, H. J. Chen, M. H. Du, L. S. Long, X. J. Kong and L. S. Zheng, *Small Methods*, 2020, 2000777.

9 E. G. Ribó, L. B. Nicola, D. L. Long and L. Cronin, *Angew. Chem., Int. Ed.*, 2022, **61**, e202201672.

10 Y. L. Wu, X. X. Li, Y. J. Qi, H. Yu, L. Jin and S. T. Zheng, *Angew. Chem., Int. Ed.*, 2018, **57**, 8572–8576.

11 J. C. Liu, Q. Han, L. J. Chen and J. W. Zhao, *CrystEngComm*, 2016, **18**, 842–862.

12 (*a*) H. Yu, Y. D. Lin, S. L. Huang, X. X. Li, C. Sun and S. T. Zheng, *Angew. Chem., Int. Ed.*, 2023, e202302111; (*b*) P. Huang, C. Qin, Z. M. Su, Y. Xing, X. L. Wang, K. Z. Shao, Y. Q. Lan and E. B. Wang, *J. Am. Chem. Soc.*, 2012, **134**, 14004–14010; (*c*) Z. K. Zhu, Y. Y. Lin, X. X. Li, D. Zhao and S. T. Zheng, *Inorg. Chem. Front.*, 2021, **8**, 1297–1302.

13 L. Zhang, L. Zhao, P. Zhang, C. Wang, S. W. Yuan and J. K. Tang, *Inorg. Chem.*, 2015, **54**, 11535–11541.

14 L. F. Wang, J. Z. Qiu, S. G. Wu, Y. C. Chen, C. J. Li, Q. W. Li, J. L. Liu and M. L. Tong, *Inorg. Chem.*, 2018, **57**, 4070–4076.

15 X. N. Yao, J. Z. Du, Y. Q. Zhang, X. B. Leng, M. W. Yang, S. D. Jiang, Z. X. Wang, Z. W. Ouyang, L. Deng, B. W. Wang and S. Gao, *J. Am. Chem. Soc.*, 2017, **139**, 373–380.

16 J. F. Wu, L. Zhao, L. Zhang, X. L. Li, M. Guo, A. K. Powell and J. K. Tang, *Angew. Chem., Int. Ed.*, 2016, **55**, 15574–15578.

17 Y. Peng and A. K. Powell, *Coord. Chem. Rev.*, 2021, **426**, 213490.

18 J. Bartolome, G. Filoti, V. Kuncser, G. Schinteie, V. Mereacre, C. E. Anson, A. K. Powell, D. Prodius and C. Turta, *Phys. Rev. B: Condens. Matter Mater. Phys.*, 2009, **80**, 014430.